Impact of Transverse Spatial-Hole Burning on Beam Quality in Large-Mode-Area Yb-Doped Fibers

Introduction

In recent years fiber lasers and amplifiers have been widely used in high-power applications such as material processing and industrial manufacturing. Their main advantages are heat-dissipation capability, broad gain bandwidth, compactness, robustness, and high efficiency. The primary limitation in their power scaling is the onset of nonlinear effects, including stimulated Brillouin scattering (SBS) and stimulated Raman scattering (SRS).[1] This limitation can be significantly mitigated by the adoption of large-mode-area (LMA) fibers due to the resulting reduction in intensity. The damage threshold is also increased for LMA fibers. However, increasing the mode area in traditional step-index fibers will introduce higher-order transverse modes and therefore degrade the beam quality. The optimization of the beam quality in LMA fibers has been a subject of intense research.[2–9]

Many designs of LMA fibers for high-power applications have been developed for beam-quality control. Design aspects have included internal structure designs such as photonic crystal fibers and helical-core fibers;[2–4] external structure designs such as coiled multimode fibers;[5] refractive-index designs such as low-numerical-aperture (NA), single-mode fibers and ring-shaped index fibers;[6,7] and gain dopant designs in multimode fibers.[8,9]

The impact, however, of transverse spatial-hole burning (TSHB) on beam quality has often been ignored. When a multimode optical beam with nonuniform transverse intensity is propagating in the fiber, the gain becomes more saturated where the intensity is highest. As the gain seen by each transverse mode changes, the net beam profile, and thus the beam quality, changes. At high powers, this effect becomes pronounced due to heavily saturated population inversion. To our knowledge, TSHB in LMA fibers has not yet been modeled.

In this article, the beam-quality factor is measured for an amplified spontaneous emission (ASE) source based on an ytterbium-doped LMA multimode fiber as a function of pump power. A localized multimode model is presented with spatially resolved gain and a modal decomposition of the optical field. Numerical simulations are performed with this localized multimode model as well as a simplified model and compared to experimental results. The comparison validates the localized model and demonstrates the impact of TSHB on beam quality.

In the following sections, (1) the experimental setup and measured results are presented; (2) a localized multimode model is introduced and the equations to calculate beam-quality factor are presented; (3) the results of numerical simulations based on this model are compared to experimental results and extrapolated to higher power; (4) the validity of a simplified model that does not include TSHB is discussed; and (5) the theoretical models are further applied to fiber amplifiers. The main conclusions are presented in the last section.

Experiment Configuration and Results

The experimental arrangement used for this work is shown schematically in Fig. 110.50. A fiber-coupled diode laser provided a maximum continuous-wave (cw) pump power of 9 W at 915 nm. The ytterbium-doped, dual-clad (YDDC) fiber was 7 m long with a core diameter of 30 μm, an inner cladding diameter of 300 μm, a core NA of 0.06, and an absorption rate of approximately 4 dB/m at 915 nm. While the back end of the fiber was angle cleaved to prevent reflection of the forward ASE, a dichroic mirror was set between two aspheric lenses to extract the backward ASE output light. A beam splitter in the output beam made it possible for the output power and the beam-quality factor (M^2 parameter) to be measured simultaneously. The ASE output power was measured by a power meter, and the beam widths (defined as the second moment) were measured by a charge-coupled-device (CCD) camera placed at different distances.[10] Using a least-squares-fitting method,[11] the beam-quality factor in the x or y direction was calculated by fitting the beam widths and distances to a polynomial:[10]

$$W^2(z) = W_0^2 + M^4\left(\frac{\lambda}{\pi W_0}\right)^2 (z - z_0)^2, \tag{1}$$

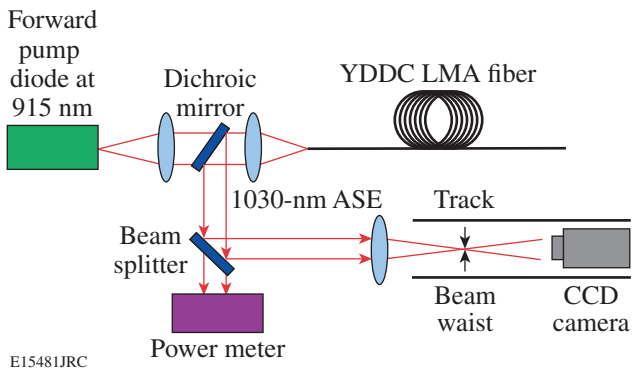

Figure 110.50
Experimental configuration of the multimode-fiber ASE source.

where $W(z)$ is the beam width at distances z, W_0 and z_0 are the respective beam width and distance at the beam waist where the beam width has a minimum, and λ is wavelength.

The ASE output power is plotted as a function of pump power in Fig. 110.51. The figure shows that output power increases exponentially and quasi-linearly when the pump power is below and above ~7 W, respectively, which means the saturation effect becomes apparent at 7-W pump power. We define this "soft" threshold as the pump threshold for saturation.

The beam-quality factor is plotted as a function of pump power in Fig. 110.52. It is instructive to note that the beam-quality factors are identical within experimental error in the x and y directions, as expected from symmetrical circular geometry. Compared with Fig. 110.51, Fig. 110.52 shows that the beam quality improves with pump power below the pump threshold for saturation and is nearly steady as the gain medium saturates. To fully understand the physics behind this beam-quality behavior, numerical simulations based on theoretical modeling have been developed.

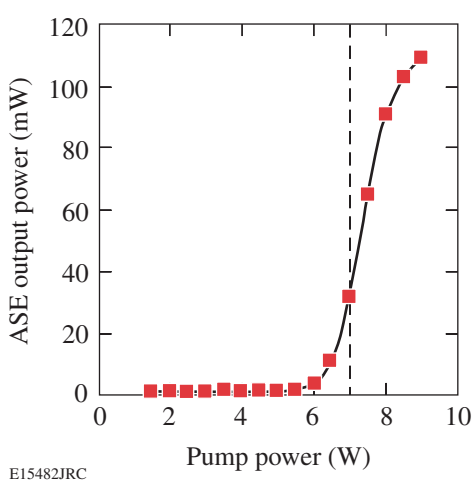

Figure 110.51
Output power versus pump power from the ASE source. The dashed vertical line is the pump threshold for saturation.

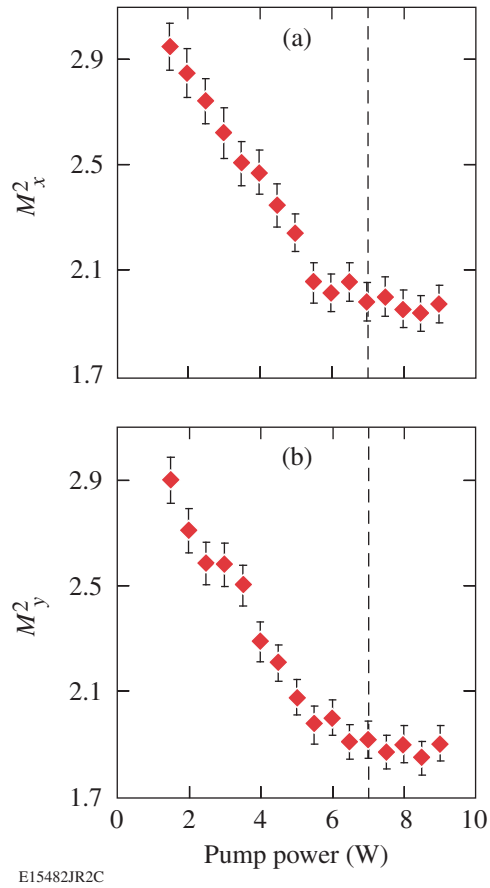

Figure 110.52
The beam-quality factor of ASE source versus pump power in the (a) x direction and (b) y direction. The dashed vertical lines are the pump thresholds for saturation.

Localized Model and Beam-Quality Factor Calculation Method

Since the beam quality is related to the modal properties of the output beam, a model that can treat multiple transverse modes is required. A multimode model has been developed for dealing with multiple spectral modes in single-spatial-mode, rare-earth–doped fibers.[12] In this work, the model is extended to multi-transverse-spatial modes in multimode fibers for the first time.

The optical power is quantized into the transverse modes of the fiber, while the population inversion retains spatial dependence. In this way, TSHB can be accounted for while retaining

the simplicity and transparency of a mode-based picture. A similar treatment has also been developed for modeling vertical-cavity, surface-emitting lasers.[13]

The two-level rate equations are given by

$$\frac{dn_2(r,\phi,z)}{dt} = \sum_k \frac{P_k(z) i_k(r,\phi)\sigma_{ak}}{h\nu_k} n_1(r,\phi,z) - \sum_k \frac{P_k(z) i_k(r,\phi)\sigma_{ek}}{h\nu_k} n_2(r,\phi,z) - \frac{n_2(r,\phi,z)}{\tau}, \quad (2)$$

$$n_t(r,\phi,z) = n_1(r,\phi,z) + n_2(r,\phi,z), \quad (3)$$

where the mode order k denotes any combination of beam propagation direction (+, –), wavelength (λ), transverse-mode order (νm), and orientation (even, odd); n_1, n_2, and n_t are ground-level, upper-level, and total ytterbium ion density, respectively, as a function of time and spatial coordinates; σ_a and σ_e are the absorption and emission cross sections of ytterbium ions, respectively; and τ is the upper-state lifetime.

$P_k(z)$, the power of the kth mode at position z in the fiber, is the integration of the light-intensity distribution $I_k(r,\phi,z)$ over the radial and azimuthal coordinates:

$$P_k(z) = \int_0^{2\pi} \int_0^{\infty} I_k(r,\phi,z) r dr d\phi. \quad (4)$$

The normalized modal-intensity distribution $i_k(r,\phi)$ is defined as

$$i_k(r,\phi) = I_k(r,\phi,z) / P_k(z) \quad (5)$$

and is determined by the spatial shape of the mode and therefore independent of z.

The terms on the right side of Eq. (2) describe the effects of absorption, stimulated emission, and spontaneous emission, respectively. Note that the interference terms are neglected in this model. This assumption is correct for transverse modes of ASE because they do not interfere with each other due to their lack of coherence. For a coherent multimode beam, this model could be modified by adding the interference terms. Mode coupling and scattering in the fiber are not considered.

In the steady-state case, the time derivative in Eq. (2) is set to zero and the inversion is solved as

$$n_2(r,\phi,z) = n_t \frac{\sum_k \frac{P_k(z) i_k(r,\phi)\sigma_{ak}}{h\nu_k}}{\frac{1}{\tau} + \sum_k \frac{P_k(z) i_k(r,\phi)(\sigma_{ak}+\sigma_{ek})}{h\nu_k}}. \quad (6)$$

The numerator accounts for small signal gain and the summation in the denominator accounts for TSHB.

The propagation equations are given by

$$\frac{dP_k(z)}{dz} = u_k \sigma_{ek}\left[P_k(z) + mh\frac{c^2}{\lambda_k^3}\Delta\lambda_k\right] \times \int_0^{2\pi}\int_0^{a} i_k(r,\phi) n_2(r,\phi,z) r dr d\phi - u_k \sigma_{ak} P_k(z) \int_0^{2\pi}\int_0^{a} i_k(r,\phi) n_1(r,\phi,z) \times r dr d\phi - u_k \alpha P_k(z). \quad (7)$$

where $u_k = 1$ for the modes traveling in the forward direction or $u_k = -1$ in the backward direction, m is the number of polarizations of each mode, $\Delta\lambda_k$ is the bandwidth, and α is the fiber-loss term. The terms on the right side of Eq. (7) describe the effects of stimulated emission, spontaneous emission, absorption, and scattering loss, respectively.

The ASE and pump have different optical properties. The modes of ASE propagate in the fiber in both directions, but the pump propagates only in the forward direction. The bandwidth of ASE is relatively narrow, so the ASE is simplified as a single spectral mode. The pump light is considered to be a single spectral mode with $\Delta\lambda_k = 0$ (no spontaneous emission at the pump wavelength).

Under the weakly guided approximation, the transverse modes of ASE can be represented by linearly polarized (LP) modes.[14] For the $LP_{\nu m}$ mode, the normalized optical intensity $i_{\nu m}(r,\phi)$ and the normalized electrical field distribution $E_{\nu m}(r,\phi)$ can be written as

$$i_{\nu m}(r,\phi) = E_{\nu m}^2(r,\phi), \tag{8}$$

$$E_{\nu m}(r,\phi) = \begin{cases} bJ_\nu(\kappa_{\nu m} r) f_\nu(\phi) & r < a_{\text{core}} \\ b\dfrac{J_\nu(\kappa_{\nu m} a_{\text{core}}) K_\nu(\gamma_{\nu m} r) f_\nu(\phi)}{K_\nu(\gamma_{\nu m} a_{\text{core}})} & r \geq a_{\text{core}} \end{cases}, \tag{9}$$

where ν and m are the azimuthal and radial mode numbers, respectively; J_ν and K_ν are the Bessel function of the first kind and modified Bessel function of the second kind, respectively; a_{core} is the radius of the core; and b is the normalization coefficient of the electrical field.

The transverse attenuation coefficient of the mode in the inner cladding $\gamma_{\nu m}$ and the transverse wave vector $\kappa_{\nu m}$ are solutions of the following system of equations:[15]

$$\kappa_{\nu m} \frac{J_{\nu-1}(\kappa_{\nu m} a_{\text{core}})}{J_\nu(\kappa_{\nu m} a_{\text{core}})} = -\gamma_{\nu m} \frac{K_{\nu-1}(\gamma_{\nu m} a_{\text{core}})}{K_\nu(\gamma_{\nu m} a_{\text{core}})}, \tag{10}$$

$$\kappa_{\nu m}^2 + \gamma_{\nu m}^2 = V^2 \big/ a_{\text{core}}^2. \tag{11}$$

The V number and NA are defined as

$$V = \frac{2\pi}{\lambda} a_{\text{core}} \text{NA}, \tag{12}$$

$$\text{NA} = \sqrt{n_{\text{core}}^2 - n_{\text{clad}}^2}, \tag{13}$$

where λ is the wavelength and n_{core} and n_{clad} are the refractive indexes in the core and cladding, respectively.

The azimuthal component $f_\nu(\phi)$ is equal to 1 for those transverse modes with zero azimuthal mode number and is given by

$$f_\nu(\phi) = \begin{cases} \cos(\nu\phi) & \text{even} \\ \sin(\nu\phi) & \text{odd} \end{cases} \tag{14}$$

for the other transverse modes with even or odd orientation.

Since the area of the inner cladding is much larger than the core, the highly multimode pump light can be simplified as one transverse mode effectively being uniformly distributed across the inner cladding and the core, which means the intensity distribution of pump I_{pump} and normalized intensity distribution of pump i_{pump} can be considered independent of radial and azimuthal coordinates. The normalized intensity distribution of the pump in inner cladding and core is then obtained from Eqs. (4) and (5) by

$$i_{\text{pump}} = \frac{1}{\pi a_{\text{clad}}^2}, \tag{15}$$

where a_{clad} is the radius of inner cladding.

The output power is the sum of the backward output power contained in each mode and is given by

$$P_{\text{output}} = \sum_{\nu,m} P_{\nu m}^-(0). \tag{16}$$

The output-fraction factor $\alpha_{\nu m}$ of $LP_{\nu m}$ mode is defined as

$$\alpha_{\nu m} = P_{\nu m}^- \big/ P_{\text{output}}. \tag{17}$$

The transverse modes with the same mode numbers but different orientations will have the same fraction factor for ASE due to symmetry.

The beam-quality factor of an optical beam can be calculated given the electrical field distribution.[16] Since the electrical field of ASE is real and symmetric at the output end and without inference, many terms in the equations to calculate the beam-quality factors vanish. The equations can then be simplified as

$$M_x^2 = 2\left[\left(\iint \sum_{\nu,m} \alpha_{\nu m} \left| \frac{\partial E_{\nu m}(r,\phi)}{\partial x} \right|^2 r dr d\phi\right) \times \left(\iint x^2 \sum_{\nu,m} \alpha_{\nu m} \left| E_{\nu m}(r,\phi) \right|^2 r dr d\phi\right)\right]^{1/2}, \tag{18}$$

$$M_y^2 = 2\left[\left(\iint \sum_{v,m} \alpha_{vm} \left| \frac{\partial E_{vm}(r,\phi)}{\partial y} \right|^2 r dr d\phi\right)\right.$$

$$\left.\times \left(\iint y^2 \sum_{v,m} \alpha_{vm} \left| E_{vm}(r,\phi) \right|^2 r dr d\phi\right)\right]^{1/2}. \quad (19)$$

Numerical Simulations and Discussions

Initial boundary conditions are needed to solve the propagation Eq. (7) and are specified at $z = 0$ and $z = L$ as

$$\begin{aligned} P^+_{\text{pump}}(0) &= P_0, \\ P^-_{\text{pump}}(L) &= 0, \\ P^+_{vm}(0) &= 0, \\ P^-_{vm}(L) &= 0, \end{aligned} \quad (20)$$

where P_0 is the forward pump power injected into the fiber and L is the length of the fiber. For ASE sources, the input signal is zero.

The parameters used in numerical simulation are listed in Table 110.VII. The emission and absorption cross sections for the fiber used in the experiment are unknown and therefore cited from another fiber with similar parameters.[17] Although the value of the bandwidth of ASE $\Delta\lambda_{\text{ASE}}$ does not affect the simulation result significantly, it is set to make the output power from simulation match that from experiment.

Given the initial boundary conditions, the propagation Eq. (7) is resolved by standard numerical integration techniques. The ASE output power and the output-fraction factors are obtained by Eqs. (16) and (17), and then the beam-quality factor is calculated by Eqs. (18) and (19). The ASE output power, the output-fraction factors, and the beam-quality factor as functions of pump power up to 25 W are calculated and plotted in Figs. 110.53, 110.54, and 110.55, respectively.

Compared with Fig. 110.51, Fig. 110.53 shows that the calculated output power has the same behavior as that from the experiment with a slightly larger value, which may result from the discrepancy between the cross sections used in simulation and experiment or over-estimation of pump power since coupling efficiency is not included in the model. The pump threshold for saturation is about 7.5 W, close to experimental results.

Figure 110.54 shows that all of the transverse modes have nearly the same output-fraction factors at very low pump power. The output-fraction factors of lower-order modes (LP_{01} and LP_{11} in this case) increase with pump power while those of higher-order modes (LP_{01}, LP_{11}, and LP_{31} in this case)

Table 110.VII: Parameters used in simulations.

Parameter	Value
n_t	1.45×10^{26} m^{-3}
λ_{ASE}	1030 nm
λ_{pump}	915 nm
$\sigma_{a\ \text{ASE}}$	4.88×10^{-26} m^2
$\sigma_{e\ \text{ASE}}$	6.24×10^{-25} m^2
$\sigma_{a\ \text{pump}}$	8.21×10^{-25} m^2
$\sigma_{e\ \text{pump}}$	3.04×10^{-26} m^2
τ	0.84 ms
$\Delta\lambda_{\text{ASE}}$	5 nm
m	2
L	7 m
a_{core}	15 μm
a_{clad}	150 μm
NA	0.06
α	0.003 m^{-1}

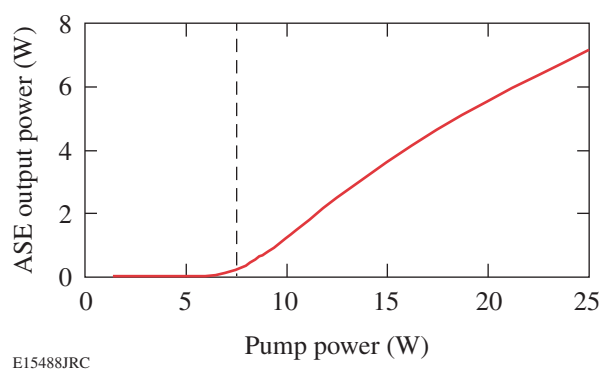

Figure 110.53
ASE output power versus pump power from the localized model. The dashed vertical line is the pump threshold for saturation.

decrease. Most importantly, the lower-order modes maximize near the pump threshold for saturation, while the higher-order modes minimize.

From Eqs. (18) and (19), it is obvious that the output-fraction factors determine the beam-quality factor since the beam-quality factor of each LP transverse mode is fixed. Generally speaking, lower-order modes have a smaller beam-quality factor, while the higher-order modes have a larger beam-quality factor.[16] So the beam-quality factor decreases, minimizes, and increases when the output fractions of lower-order modes increase, maximize, and decrease, respectively.

This behavior is manifest in Fig. 110.55, which shows that the beam-quality factor decreases with increasing pump power below pump threshold for saturation as shown experimentally in Fig. 110.52. The calculation further shows that the nearly steady part near pump threshold for saturation in Fig. 110.52 is a minimum. The behavior of the beam-quality factor follows directly from the behavior of output-fraction factors as shown in Fig. 110.55. The output-fraction factors, and thus the beam-quality factor, are determined by how much gain is experienced by each transverse mode, which depends on the overlap of mode field distribution and population inversion distribution.

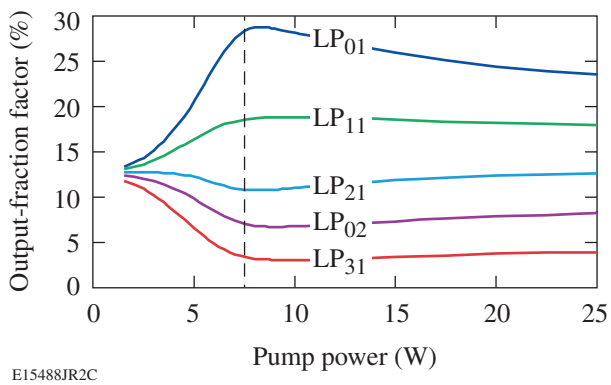

Figure 110.54
Output-fraction factors of LP fiber modes versus pump power from the localized model. The dashed vertical line is the pump threshold for saturation.

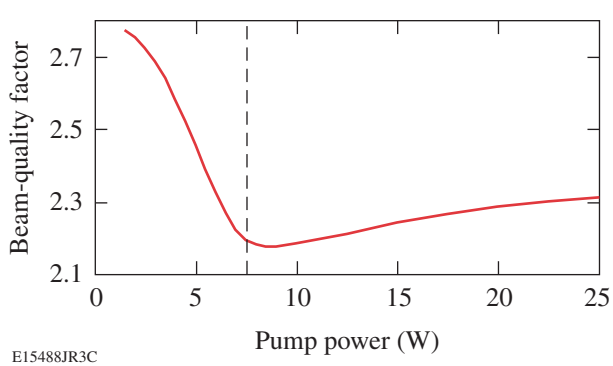

Figure 110.55
Beam-quality factor versus pump power from the localized model. The dashed vertical line is the pump threshold for saturation.

The upper-level dopant distribution across the injection fiber end for various pump powers is plotted in Fig. 110.56. When 5-W pump power is below the pump threshold for saturation, the population inversion is nearly uniform across the core, so the modal gain is nearly proportional to the fraction of the mode in the core. Since the fields of lower-order modes are more confined in the core, the lower-order modes have larger gain than the higher-order modes, as shown in Table 110.VIII. In this small-signal regime, the power in the modes with larger gain increases faster than in the modes with smaller gain. Therefore, the output-fraction factors of lower-order modes increase and the beam quality improves.

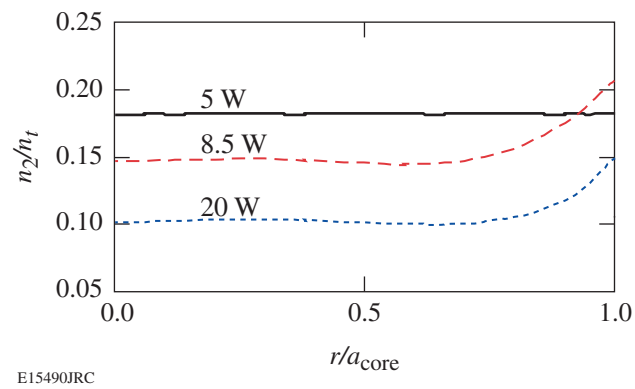

Figure 110.56
Upper-level dopant distributions with various pump powers across the injection fiber end.

Table 110.VIII: The ratio of the gain seen by other transverse modes to the gain seen by the fundamental mode with 5-W pump power.

Mode	$g_{LP_{vm}}/g_{LP_{01}}$
LP_{11}	95.6%
LP_{21}	89.8%
LP_{02}	85.4%
LP_{31}	78.0%

Above the pump threshold for saturation, TSHB is shown in the upper-level dopant distribution with 8.5- and 20-W pump power in Fig. 110.56, where the gain profile is much more saturated in the center of the core than on the edge. Since lower-order modes are more concentrated in the center of the core, the gain of lower-order modes decreases relative to the gain of higher-order modes. In the saturation region, the faster the gain in the modes decreases, the slower the power in the modes increases. So under the impact of TSHB the output-fraction factors of lower-order modes decrease and the beam quality degrades.

The Validity of a Simplified Model

The rate and propagation equations are often simplified by replacing transverse space integrals with overlap integrals, especially in single-mode fibers.[18] The validity of such simplification in multimode fibers is discussed below.

The rate equations of such a simplified model are given by

$$\frac{dn_2(z)}{dt} = \sum_k \frac{P_k(z)\Gamma_k \sigma_{ak}}{h\nu_k A} n_1(z) - \sum_k \frac{P_k(z)\Gamma_k \sigma_{ek}}{h\nu_k A} n_2(z) - \frac{n_2(z)}{\tau}, \tag{21}$$

$$n_t(z) = n_1(z) + n_2(z), \tag{22}$$

where n_1 and n_2 represent average ground-level and upper-level ytterbium ion density across the fiber cross section, respectively, A is the area of the core cross section, and Γ_k is the overlap integral between the mode and dopants.

The overlap integral of ASE modes is given by

$$\Gamma_{vm} = \frac{\int_0^{2\pi}\int_0^{\infty} i_{vm}(r,\phi) n_t(r,\phi,z) r dr d\phi}{\int_0^{2\pi}\int_0^{\infty} n_t(r,\phi,z) r dr d\phi}. \tag{23}$$

If the dopant is distributing uniformly in the fiber core, Γ_{vm} depends only on the mode field and can be simplified as

$$\Gamma_{vm} = \int_0^{2\pi}\int_0^{a_{core}} i_{vm}(r,\phi) r dr d\phi. \tag{24}$$

The overlap integral of pump is given by

$$\Gamma_{\text{pump}} = a_{\text{core}}^2 \big/ a_{\text{clad}}^2. \tag{25}$$

In the steady-state case, n_2 is solved as

$$n_2(z) = n_t \frac{\sum_k \frac{P_{k(z)}\Gamma_k \sigma_{ak}}{h\nu_k A}}{\frac{1}{\tau} + \sum_k \frac{P_{k(z)}\Gamma_k(\sigma_{ak}+\sigma_{ek})}{h\nu_k A}}. \tag{26}$$

Since the upper-level dopant distribution depends only on the longitudinal coordinate z and is independent of radial and azimuthal coordinates, TSHB is not included in the simplified model. The saturation effect is included as an averaged level across the core.

The simplified propagation equation is given by

$$\frac{dP_k(z)}{dz} = u_k \sigma_{ek}\left[P_k(z) + mh\frac{c^2}{\lambda_k^3}\Delta\lambda_k\right]\Gamma_k n_2(z) - u_k \sigma_{ak} P_k(z)\Gamma_k n_1(z) - u_k \alpha P_k(z). \tag{27}$$

Given the same initial boundary conditions as Eq. (20), the propagation equation (27) is resolved. The output power as a function of pump power is the same in the simplified model as the localized model; however, the modal properties are significantly different. The output-fraction factors and beam-quality factor as functions of pump power up to 25 W in the simplified model compared to the localized model are shown in Figs. 110.57 and 110.58.

Figure 110.57 shows that the output-fraction factors in the simplified model are the same as those in the localized model when the pump power is below the pump threshold for saturation. However, the output-fraction factors of lower-order modes in the simplified model keep increasing beyond the pump threshold for saturation, becoming constant after 15 W. Similarly, Fig. 110.58 shows that the beam-quality factor in the

simplified model is the same as that in the localized model at pump power below pump threshold for saturation. Above the pump threshold for saturation, however, the beam-quality factor in the simplified model keeps decreasing until 15 W and then becomes constant.

The behaviors of output-fraction factors and beam-quality factor are consistent and can be explained as follows: In the simplified model, the gain seen by each transverse mode is always proportional to the fraction of the mode in the core, so the simplified model gives the same simulation results as the localized model below the pump threshold of saturation. Above the pump threshold for saturation, the gain of each mode decreases at the same rate, so the power in each mode increases at the same rate. Therefore, the output-fraction factor of each mode becomes constant, as does the beam-quality factor.

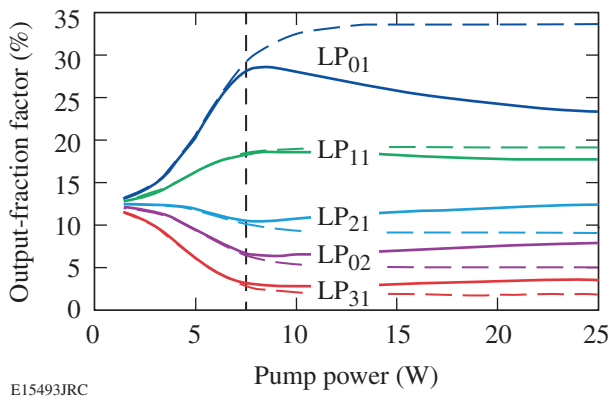

Figure 110.57
Output-fraction factors of LP fiber modes versus pump power from localized (solid) and simplified (dashed) models. The dashed vertical line is the pump threshold for saturation.

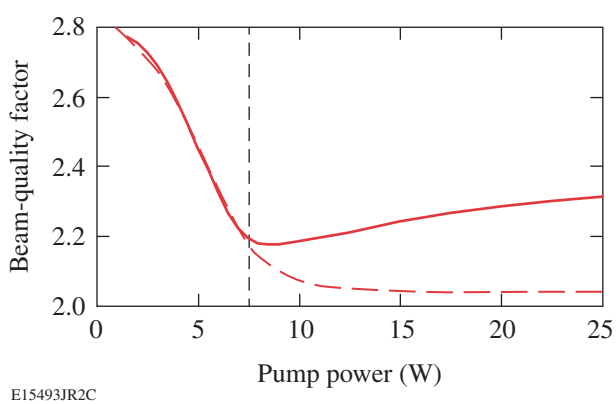

Figure 110.58
Beam-quality factor versus pump power from localized (solid) and simplified (dashed) models. The dashed vertical line is the pump threshold for saturation.

The beam-quality factors from simulation results of both models and the experimental results near pump threshold for saturation are compared in Fig. 110.59. Figure 110.59 shows that the beam-quality factor of the simplified model does not plateau like the experiment data, but the localized model predicts this behavior. The failure to show the minimum of beam-quality factor near pump threshold for saturation proves that the simplified model is not valid and TSHB is required to model LMA multimode fibers when dealing with beam quality.

Fiber Amplifiers

Fiber amplifiers are more important than ASE sources in high-power applications of LMA fibers. As mentioned in **Localized Model and Beam-Quality Factor Calculation Method** (p. 121), the localized model assumes no interference, which is true for an optical beam from incoherent sources like ASE, but not for coherent sources like fiber amplifiers. While the equations could be easily modified to include the interference terms, the relative phases between modes create a large additional parameter space that would require exploration. The calculations that follow neglect these interference terms since the additional complication does not aid in underscoring the importance of TSHB.

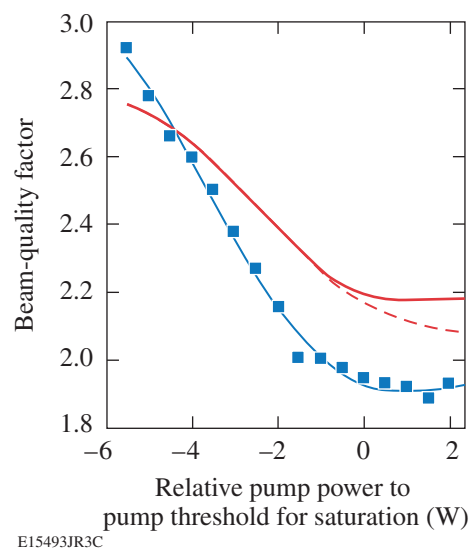

Figure 110.59
Beam-quality factor versus relative pump power to pump threshold for saturation from localized (solid) and simplified (dashed) models as well as experimental measurements (squares with solid-line fit).

For the purpose of simplicity, only the LP_{01} and LP_{11} modes are assumed to be coupled into the fiber amplifier. The power contained in the LP_{11} mode is assumed to be evenly distributed in two orientations.

The initial boundary conditions are changed to

$$\begin{aligned} &P^{+}_{\text{pump}}(0) = P_0, \\ &P^{-}_{\text{pump}}(L) = 0, \\ &P^{+}_{01}(0) = P_s\chi, \\ &P^{+}_{11}(0) = P_s(1-\chi), \\ &P^{+}_{vm}(0) = 0, \text{otherwise} \\ &P^{-}_{vm}(L) = 0, \end{aligned} \tag{28}$$

where P_s is the total signal power and χ is the input-fraction factor of the LP_{01} mode.

The normalized electrical field distribution of the output beam can be written as

$$E(r,\phi) = \sum_{v,m} \sqrt{\alpha_{vm}}\, E_{vm}(r,\phi) e^{-i\beta_{vm}L}, \tag{29}$$

where the propagation coefficient β_{vm} is given by[15]

$$\beta^2_{vm} = \left(\frac{2\pi}{\lambda}\right)^2 n^2_{\text{core}} - \kappa^2_{vm}. \tag{30}$$

In this form, modal dispersion is included. No initial phase difference is considered between the modes since the two modes are assumed to be excited by a single-mode input beam (for example, by misalignment).

Since the output beam is real and symmetrical, the equations to calculate the beam-quality factors in Ref. 16 can be simplified as

$$M^2_x = 2\sqrt{\left[\iint \left|\frac{\partial E(r,\phi)}{\partial x}\right|^2\right]\left[\iint x^2 \left|E(r,\phi)\right|^2 r dr d\phi\right]}, \tag{31}$$

$$M^2_y = 2\sqrt{\left[\iint \left|\frac{\partial E(r,\phi)}{\partial y}\right|^2\right]\left[\iint y^2 \left|E(r,\phi)\right|^2 r dr d\phi\right]}. \tag{32}$$

The new parameters used in the simulation and those that differ from Table 110.VII are listed in Table 110.IX: λ_s is the wavelength of the signal, $\Delta\lambda_{\text{ASE}}$ is set to be the same as the bandwidth of the signal, and P_0 is set far above the pump threshold for saturation, which is true in most high-power applications.

Table 110.IX: New and changed parameters used in simulations.

Parameter	Value
λ_S	1030 nm
P_s	10 W
n_{core}	1.5
$\Delta\lambda_{\text{ASE}}$	0.1 nm
P_0	1.5 kW

The calculations show that the output power is nearly the same in both models and does not change as the input-fraction factor. For both models, the output-fraction factor of the fundamental mode and the beam-quality factor are calculated as a function of the input-fraction factor of the LP_{01} mode from 0.5 to 1 (shown in Figs. 110.60 and 110.61).

Figure 110.60 shows that the output-fraction factor of the fundamental mode in the localized model is smaller than the corresponding input-fraction factor, while the output-fraction factor of the fundamental mode in the simplified model is larger. These behaviors can be explained as follows: The pump power used in the simulations is well above pump threshold for saturation. In the localized model, the gain of fundamental mode is less than that of the LP_{11} mode due to the effect of TSHB. Therefore, the fundamental mode is amplified less than the LP_{11} mode, leading to a smaller output-fraction factor of the fundamental mode. In the simplified model, however, TSHB is ignored and the gain of fundamental mode is always larger than that of the LP_{11} mode. In this case, the fundamental mode is always amplified more than the LP_{11} mode, leading to a larger output-fraction factor of the fundamental mode.

Figure 110.61 shows that the beam-quality factor in the simplified model is underestimated by as much as 15% compared to the localized model due to underestimation of the output-fraction factor of the fundamental mode. This significant difference underscores the importance of TSHB on beam quality in LMA fiber amplifiers for high-power applications.

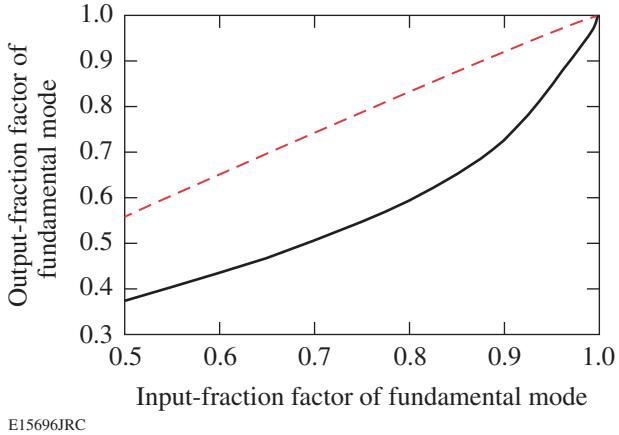

Figure 110.60
Output-fraction factors of the fundamental mode versus input-fraction factors of the fundamental mode from localized (solid) and simplified (dashed) models.

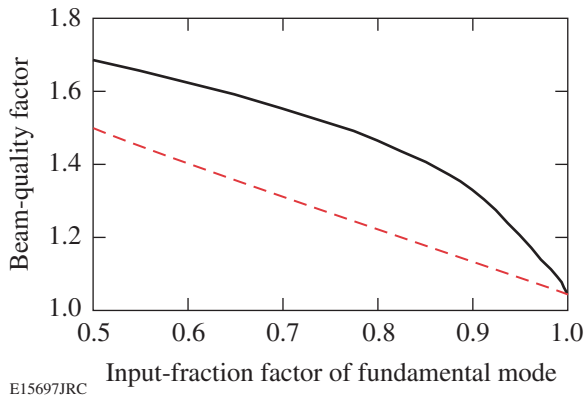

Figure 110.61
Beam-quality factors versus pump power from localized (solid) and simplified (dashed) models.

Conclusions

In conclusion, the importance of TSHB on the beam quality of LMA multimode fibers was revealed through measurements and simulations. The measured beam-quality factor decreases until the gain becomes saturated in an ASE source based on an ytterbium-doped, large-mode-area, multimode fiber. Numerical simulation trends based on a model using spatially resolved gain and transverse-mode decomposition of the optical field agree with the experimental results. A simplified model without TSHB is shown not fit to predict the observed behavior of beam quality in LMA fibers, especially at high powers. A comparison of both models shows that TSHB is also critical for properly modeling beam quality in LMA fiber amplifiers.

ACKNOWLEDGMENT

This work was supported by the U.S. Department of Energy Office of Inertial Confinement Fusion under Cooperative Agreement No. DE-FC52-92SF19460, the University of Rochester, and the New York State Energy Research and Development Authority. The support of DOE does not constitute an endorsement by DOE of the views expressed in this article.

REFERENCES

1. G. P. Agrawal, *Nonlinear Fiber Optics* (Academic Press, Boston, 1989).
2. T. A. Birks, J. C. Knight, and P. St. J. Russell, Opt. Lett. **22**, 961 (1997).
3. P. Wang *et al.*, Opt. Lett. **31**, 226 (2006).
4. Z. Jiang and J. R. Marciante, J. Opt. Soc. Am. B **23**, 2051 (2006).
5. P. Koplow, D. A. V. Kliner, and L. Goldberg, Opt. Lett. **25**, 442 (2000).
6. D. Taverner *et al.*, Opt. Lett. **22**, 378 (1997).
7. H. L. Offerhaus *et al.*, Opt. Lett. **23**, 1683 (1998).
8. J. M. Sousa and O. G. Okhotnikov, Appl. Phys. Lett. **74**, 1528 (1999).
9. J. R. Marciante, presented at ASSP 2007, Vancouver, Canada, 28–31 January 2007.
10. A. E. Siegman, in *Diode Pumped Solid State Lasers: Applications and Issues*, edited by M. W. Dowley, OSA TOPS, Vol. 17 (Optical Society of America, Washington, DC, 1998), pp. 184–199.
11. P. R. Bevington, *Data Reduction and Error Analysis for the Physical Sciences* (McGraw-Hill, New York, 1969), pp. 135–155.
12. C. R. Giles and E. Desurvire, J. Lightwave Technol. **9**, 271 (1991).
13. J. Y. Law, IEEE Photonics Technol. Lett. **9**, 437 (1997).
14. D. Gloge, Appl. Opt. **10**, 2252 (1971).
15. C. R. Pollock, *Fundamentals of Optoelectronics* (Irwin, Chicago, 1995).
16. H. Yoda *et al.*, J. Lightwave Technol. **24**, 1350 (2006).
17. J. R. Marciante and J. D. Zuegel, Appl. Opt. **45**, 6798 (2006).
18. Hardy, J. Lightwave Technol. **16**, 1865 (1998).